LECTURE 18: Horn Antennas

(*Rectangular horn antennas. Circular apertures.*)

1 Rectangular Horn Antennas

Horn antennas are popular in the microwave bands (above 1 GHz). Horns provide high gain, low VSWR (with waveguide feeds), relatively wide bandwidth, and they are not difficult to make. There are three basic types of rectangular horns.

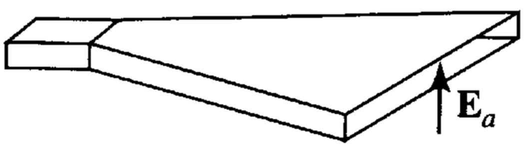

(*a*) *H*-plane sectoral horn.

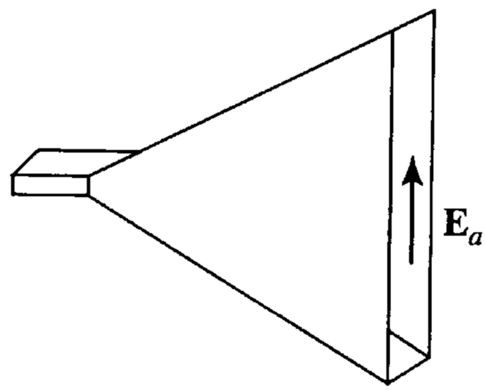

(*b*) *E*-plane sectoral horn.

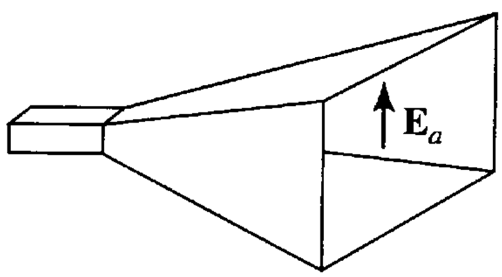

(*c*) Pyramidal horn.

[Balanis]

The horns can be also flared exponentially. This provides better impedance match in a broader frequency band. Such horns are more difficult to make, which means higher cost.

The rectangular horns are ideally suited for rectangular waveguide feeds. The horn acts as a gradual transition from a waveguide mode to a free-space mode of the EM wave. When the feed is a cylindrical waveguide, the antenna is usually a ***conical horn***.

Why is it necessary to consider the horns separately instead of applying the theory of waveguide aperture antennas (see Lecture 17) directly? It is because the so-called ***phase error*** occurs due to the difference between the lengths from the center of the feed to the center of the horn aperture and the horn edge. The field does not have the same phase across the horn aperture. This makes the uniform-phase aperture results invalid for the horns.

1.1 The *H*-plane sectoral horn

The geometry and the respective parameters shown in the figure below are used in the subsequent analysis. The two required dimensions for the construction of the horn are A and R_H.

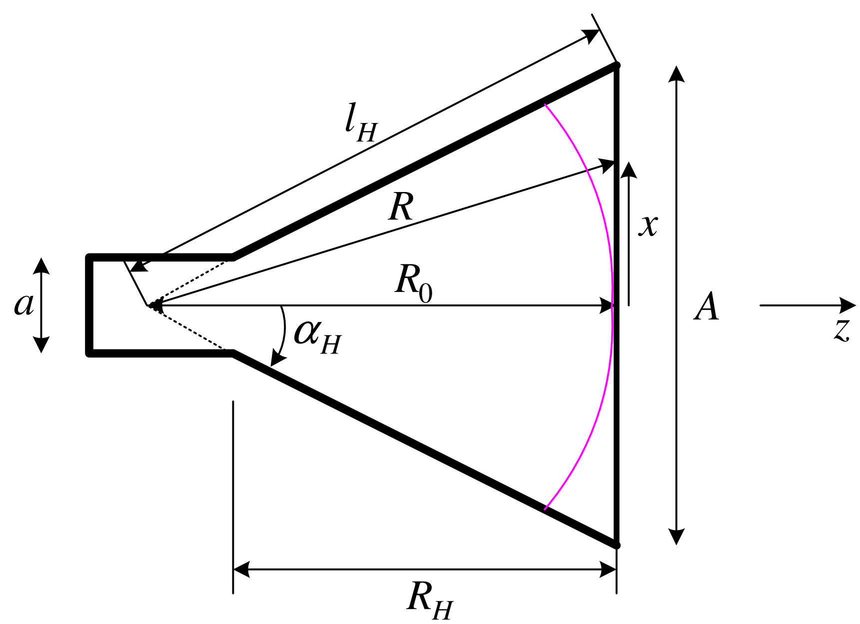

H-PLANE (*X*-*Z*) CUT OF AN *H*-PLANE SECTORAL HORN

$$l_H^2 = R_0^2 + \left(\frac{A}{2}\right)^2, \tag{18.1}$$

$$\alpha_H = \arctan\left(\frac{A}{2R_0}\right), \tag{18.2}$$

$$R_H = (A-a)\sqrt{\left(\frac{l_H}{A}\right) - \frac{1}{4}}. \tag{18.3}$$

The tangential field arriving at the input of the horn is composed of the transverse field components of the waveguide dominant mode TE_{10}:

$$\left| \begin{array}{l} E_y(x) = E_0 \cos\left(\dfrac{\pi}{a} x\right) e^{-j\beta_g z} \\ H_x(x) = -E_y(x) / Z_w \end{array} \right. \tag{18.4}$$

where

$Z_w = \dfrac{\eta}{\sqrt{1-\left(\dfrac{\lambda_0}{2a}\right)^2}}$ is the wave impedance of the TE_{10} waveguide mode,

$\beta_g = \beta_0 \sqrt{1-\left(\dfrac{\lambda_0}{2a}\right)^2}$ is the phase constant of the guided TE_{10} mode.

Here, $\beta_0 = \omega\sqrt{\mu\varepsilon} = 2\pi / \lambda_0$, and λ_0 is the free-space wavelength. The field that is illuminating the aperture of the horn can be approximated as a spatially expanded version of the waveguide field. Note that the wave impedance of the flared waveguide (the horn) gradually approaches the intrinsic impedance of open space η, as A (the H-plane width) increases.

The complication in the analysis arises from the fact that the waves arriving at the horn aperture are ***not in phase*** due to the different path lengths from the horn apex. The aperture phase variation is given by

$$e^{-j\beta(R-R_0)}. \tag{18.5}$$

Since the aperture is not flared in the y-direction, the phase is uniform along y. We first approximate the path of the wave in the horn:

$$R = \sqrt{R_0^2 + x^2} = R_0 \sqrt{1+\left(\frac{x}{R_0}\right)^2} \approx R_0 \left[1 + \frac{1}{2}\left(\frac{x}{R_0}\right)^2\right]. \tag{18.6}$$

The last approximation holds if $x \ll R_0$, or $A/2 \ll R_0$. Then, we can assume that

$$R - R_0 \approx \frac{1}{2}\frac{x^2}{R_0}. \tag{18.7}$$

Using (18.7), the field at the aperture is approximated as

$$E_{a_y}(x) \approx E_0 \cos\left(\pi x / A\right) e^{-j\frac{\beta}{2R_0}x^2}. \tag{18.8}$$

The field at the aperture plane outside the aperture is assumed equal to zero. The field expression (18.8) is substituted in the integral for I_y^E (see Lecture 17):

$$I_y^E(\theta,\varphi) = \iint_{S_A} E_{a_y}(x', y') e^{j\beta(x'\sin\theta\cos\varphi + y'\sin\theta\sin\varphi)} dx'dy', \tag{18.9}$$

$$I_y^E(\theta,\varphi) = E_0 \underbrace{\int_{-A/2}^{+A/2} \cos\left(\frac{\pi}{A}x'\right) e^{-j\frac{\beta}{2R_0}x'^2} e^{j\beta x'\sin\theta\cos\varphi} dx'}_{\sim I(\theta,\varphi)} \times \int_{-b/2}^{+b/2} e^{j\beta y'\sin\theta\sin\varphi} dy'. \tag{18.10}$$

The second integral has been already solved in Lecture 17. The first integral is cumbersome and the final result only is given below:

$$I_y^E(\theta,\varphi) = E_0 \left[\frac{1}{2}\sqrt{\frac{\pi R_0}{\beta}} \cdot I(\theta,\varphi)\right] \times \left[b\frac{\sin\left(0.5\beta b \cdot \sin\theta \cdot \sin\varphi\right)}{\left(0.5\beta b \cdot \sin\theta \cdot \sin\varphi\right)}\right], \tag{18.11}$$

where

$$\begin{aligned} I(\theta,\varphi) = {} & e^{j\frac{R_0}{2\beta}\left(\beta\sin\theta\cos\varphi + \frac{\pi}{A}\right)^2} \cdot \left[C(s_2') - jS(s_2') - C(s_1') + jS(s_1')\right] \\ & + e^{j\frac{R_0}{2\beta}\left(\beta\sin\theta\cos\varphi - \frac{\pi}{A}\right)^2} \cdot \left[C(t_2') - jS(t_2') - C(t_1') + jS(t_1')\right] \end{aligned} \tag{18.12}$$

and

$$s_1' = \sqrt{\frac{1}{\pi\beta R_0}}\left(-\frac{\beta A}{2} - R_0\beta u - \frac{\pi R_0}{A}\right);$$

$$s_2' = \sqrt{\frac{1}{\pi\beta R_0}}\left(+\frac{\beta A}{2} - R_0\beta u - \frac{\pi R_0}{A}\right);$$

$$t_1' = \sqrt{\frac{1}{\pi\beta R_0}}\left(-\frac{\beta A}{2} - R_0\beta u + \frac{\pi R_0}{A}\right);$$

$$t_2' = \sqrt{\frac{1}{\pi\beta R_0}}\left(+\frac{\beta A}{2} - R_0\beta u + \frac{\pi R_0}{A}\right);$$

$$u = \sin\theta\cos\varphi.$$

$C(x)$ and $S(x)$ are Fresnel integrals, which are defined as

$$C(x)=\int_0^x \cos\left(\frac{\pi}{2}\tau^2\right)d\tau; \quad C(-x)=-C(x),$$
$$S(x)=\int_0^x \sin\left(\frac{\pi}{2}\tau^2\right)d\tau; \quad S(-x)=-S(x). \tag{18.13}$$

More accurate evaluation of $I_y^E(\theta,\varphi)$ is obtained if the approximation in (18.6) is not made, and E_{a_y} is substituted in (18.9) as

$$E_{a_y}(x)=E_0\cos\left(\frac{\pi}{A}x\right)e^{-j\beta\left(\sqrt{R_0^2+x^2}-R_0\right)}=E_0e^{+j\beta R_0}\cos\left(\frac{\pi}{A}x\right)e^{-j\beta\sqrt{R_0^2+x^2}}. \tag{18.14}$$

The far field can be calculated from $I_y^E(\theta,\varphi)$ as (see Lecture 17):

$$E_\theta = j\beta\frac{e^{-j\beta r}}{4\pi r}(1+\cos\theta)\sin\varphi\cdot I_y^E(\theta,\varphi),$$
$$E_\varphi = j\beta\frac{e^{-j\beta r}}{4\pi r}(1+\cos\theta)\cos\varphi\cdot I_y^E(\theta,\varphi), \tag{18.15}$$

or

$$\mathbf{E}=j\beta E_0 b\sqrt{\frac{\pi R_0}{\beta}}\frac{e^{-j\beta r}}{4\pi r}\left(\frac{1+\cos\theta}{2}\right)\left[\frac{\sin(0.5\beta b\cdot\sin\theta\cdot\sin\varphi)}{(0.5\beta b\cdot\sin\theta\cdot\sin\varphi)}\right]\times$$
$$I(\theta,\varphi)\left(\hat{\boldsymbol{\theta}}\sin\varphi+\hat{\boldsymbol{\varphi}}\cos\varphi\right). \tag{18.16}$$

The amplitude pattern of the *H*-plane sectoral horn is obtained as

$$\bar{E}(\theta,\varphi)=\left(\frac{1+\cos\theta}{2}\right)\cdot\left[\frac{\sin(0.5\beta b\cdot\sin\theta\cdot\sin\varphi)}{(0.5\beta b\cdot\sin\theta\cdot\sin\varphi)}\right]\cdot I(\theta,\varphi). \tag{18.17}$$

Principal-plane patterns

***E*-plane** ($\varphi=90°$): $F_E(\theta)=\left(\frac{1+\cos\theta}{2}\right)\left[\frac{\sin(0.5\beta b\cdot\sin\theta)}{(0.5\beta b\cdot\sin\theta)}\right]$ (18.18)

The second factor in (18.18) is dominant and it is identical to the second factor of the pattern of a slit of width *b* (along the *y*-axis).

***H*-plane** ($\varphi = 0°$):

$$F_H(\theta) = \left(\frac{1+\cos\theta}{2}\right) \cdot f_H(\theta) = \left(\frac{1+\cos\theta}{2}\right) \cdot \frac{I(\theta, \varphi = 0°)}{I(\theta = 0°, \varphi = 0°)} \tag{18.19}$$

The H-plane pattern in terms of the $I(\theta, \varphi)$ integral is an approximation, which is a consequence of the phase approximation made in (18.7). Accurate value for $f_H(\theta)$ is found by integrating numerically the field as given in (18.14), i.e.,

$$f_H(\theta) \propto \int_{-A/2}^{+A/2} \cos\left(\frac{\pi x'}{A}\right) e^{-j\beta\sqrt{R_0^2 + x'^2}} e^{j\beta x' \sin\theta} dx'. \tag{18.20}$$

E- AND H-PLANE PATTERN OF H-PLANE SECTORAL HORN

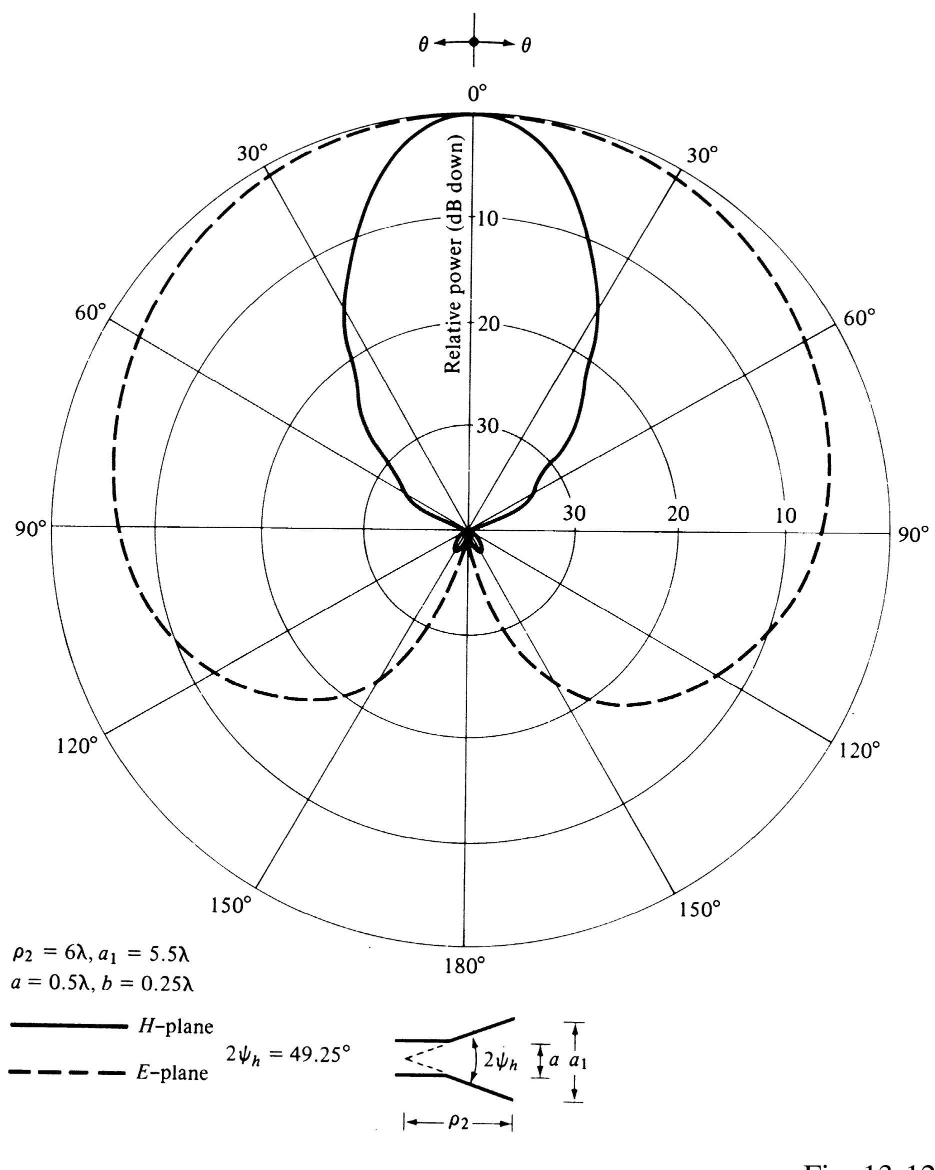

Fig. 13-12, Balanis, p. 674

The directivity of the H-plane sectoral horn is calculated by the general directivity expression for apertures (for derivation, see Lecture 17):

$$D_0 = \frac{4\pi}{\lambda^2} \cdot \frac{\left| \iint_{S_A} \mathbf{E}_a ds' \right|^2}{\iint_{S_A} |\mathbf{E}_a|^2 ds'}. \quad (18.21)$$

The integral in the denominator is proportional to the total radiated power,

$$2\eta\Pi_{rad} = \iint_{S_A} |\mathbf{E}_a|^2 ds' = \int_{-b/2}^{+b/2} \int_{-A/2}^{+A/2} |E_0|^2 \cos^2\left(\frac{\pi}{A}x'\right) dx'dy' = |E_0|^2 \frac{Ab}{2}. \quad (18.22)$$

In the solution of the integral in the numerator of (18.21), if the field is substituted with its phase approximation in (18.8), the result for the directivity of the H-plane horn is

$$\boxed{D_H = \frac{b}{\lambda}\frac{32}{\pi}\left(\frac{A}{\lambda}\right)\varepsilon_{ph}^H = \frac{4\pi}{\lambda^2}\varepsilon_t \varepsilon_{ph}^H (Ab),} \quad (18.23)$$

where

$$\varepsilon_t = \frac{8}{\pi^2};$$

$$\varepsilon_{ph}^H = \frac{\pi^2}{64t}\left\{\left[C(p_1) - C(p_2)\right]^2 + \left[S(p_1) - S(p_2)\right]^2\right\};$$

$$p_1 = 2\sqrt{t}\left[1 + \frac{1}{8t}\right], \quad p_2 = 2\sqrt{t}\left[-1 + \frac{1}{8t}\right];$$

$$t = \frac{1}{8}\left(\frac{A}{\lambda}\right)^2 \frac{1}{R_0/\lambda}.$$

The factor ε_t explicitly shows the aperture efficiency associated with the aperture cosine taper. The factor ε_{ph}^H is the aperture efficiency associated with the aperture phase distribution.

A family of universal directivity curves is given below. From these curves, it is obvious that for a given axial length R_0 and at a given wavelength, there is an optimal aperture width A corresponding to the maximum directivity.

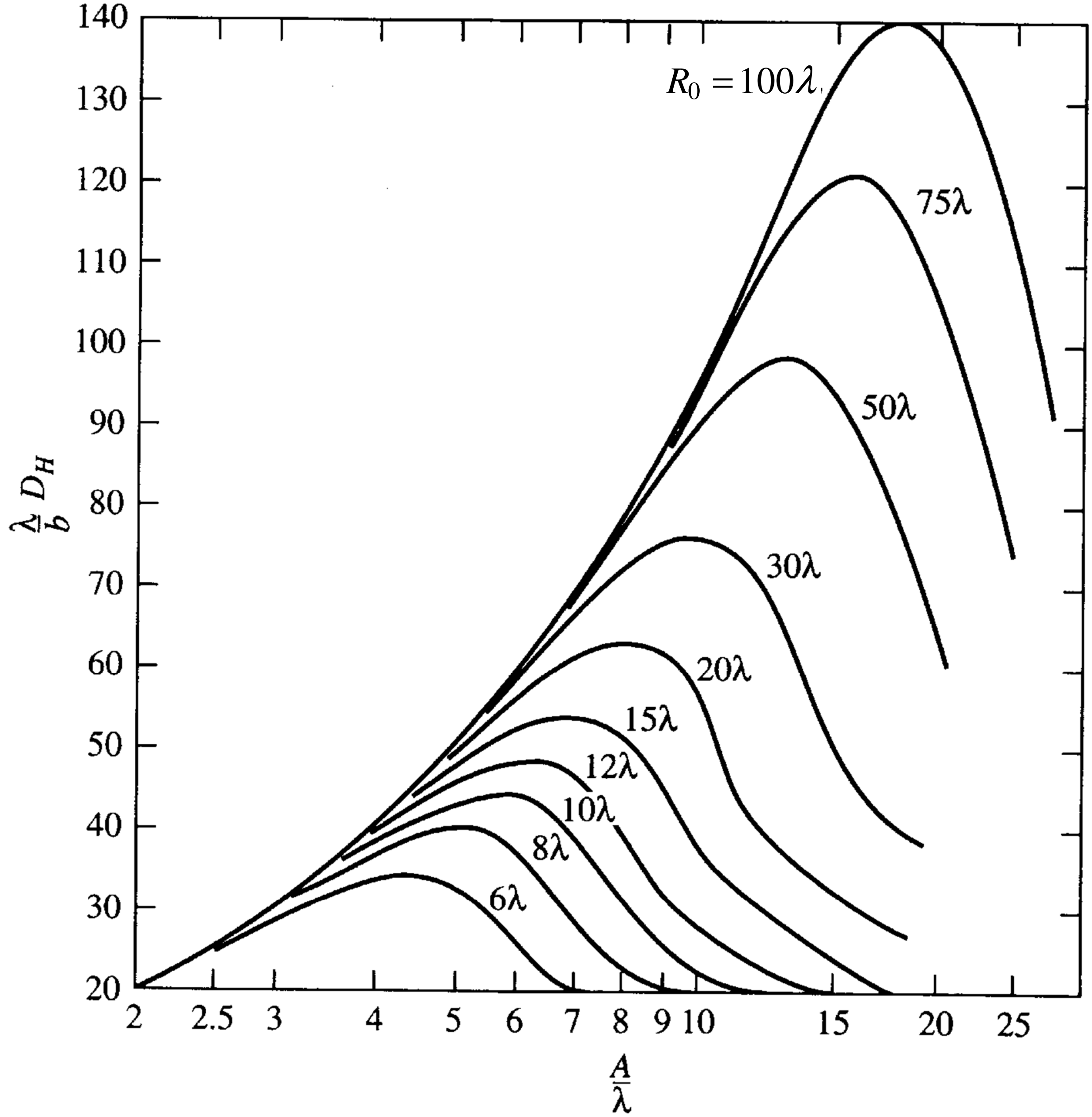

[Stutzman&Thiele, *Antenna Theory and Design*]

It can be shown that the optimal directivity is obtained if the relation between A and R_0 is

$$A = \sqrt{3\lambda R_0}, \tag{18.24}$$

or

$$\frac{A}{\lambda} = \sqrt{3\frac{R_0}{\lambda}}. \tag{18.25}$$

1.2 The *E*-plane sectoral horn

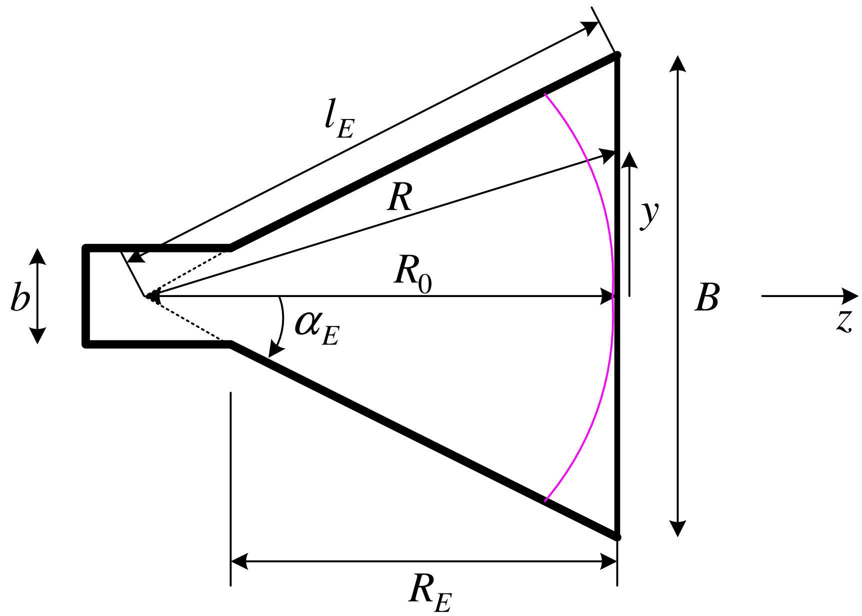

E-plane (*y*-*z*) cut of an *E*-plane sectoral horn

The geometry of the *E*-plane sectoral horn in the *E*-plane (*y*-*z* plane) is analogous to that of the *H*-plane sectoral horn in the *H*-plane. The analysis follows the same steps as in the previous section. The field at the aperture is approximated by [compare with (18.8)]

$$E_{a_y} = E_0 \cos\left(\frac{\pi}{a} x\right) e^{-j\frac{\beta}{2R_0} y^2} . \tag{18.26}$$

Here, the approximations

$$R = \sqrt{R_0^2 + y^2} = R_0 \sqrt{1 + \left(\frac{y}{R_0}\right)^2} \approx R_0 \left[1 + \frac{1}{2}\left(\frac{y}{R_0}\right)^2\right] \tag{18.27}$$

and

$$R - R_0 \approx \frac{1}{2} \frac{y^2}{R_0} \tag{18.28}$$

are made, which are analogous to (18.6) and (18.7).

The radiation field is obtained as

$$\mathbf{E} = j\beta E_0 \frac{4a}{\pi}\sqrt{\frac{\pi R_0}{\beta}}\frac{e^{-j\beta r}}{4\pi r} e^{j\left(\frac{\beta R_0}{2}\right)\left(\frac{\beta B}{2}\sin\theta\sin\varphi\right)^2} \cdot \left(\hat{\boldsymbol{\theta}}\sin\varphi + \hat{\boldsymbol{\varphi}}\cos\varphi\right)$$

$$\times\frac{(1+\cos\theta)}{2}\frac{\cos\left(\dfrac{\beta a}{2}\sin\theta\cos\varphi\right)}{\left[1-\left(\dfrac{\beta a}{2}\sin\theta\cos\varphi\right)^2\right]}\left[C(r_2)-jS(r_2)-C(r_1)+jS(r_1)\right]. \quad (18.29)$$

The arguments of the Fresnel integrals used in (18.29) are

$$r_1 = \sqrt{\frac{\beta}{\pi R_0}}\left(-\frac{B}{2} - R_0\frac{\beta B}{2}\sin\theta\sin\varphi\right),$$
$$r_2 = \sqrt{\frac{\beta}{\pi R_0}}\left(+\frac{B}{2} - R_0\frac{\beta B}{2}\sin\theta\sin\varphi\right). \quad (18.30)$$

Principal-plane patterns

The **normalized *H*-plane pattern** is found by substituting $\varphi = 0$ in (18.29):

$$\bar{H}(\theta) = \left(\frac{1+\cos\theta}{2}\right)\times\frac{\cos\left(\dfrac{\beta a}{2}\sin\theta\right)}{1-\left(\dfrac{\beta a}{2}\sin\theta\right)^2}. \quad (18.31)$$

The second factor in this expression is the pattern of a uniform-phase cosine-amplitude tapered line source.

The **normalized *E*-plane pattern** is found with $\varphi = 90°$ substituted in (18.29):

$$\bar{E}(\theta) = \frac{(1+\cos\theta)}{2}\left|f_E(\theta)\right| = \frac{(1+\cos\theta)}{2}\sqrt{\frac{\left[C(r_2)-C(r_1)\right]^2+\left[S(r_2)-S(r_1)\right]^2}{4\left[C^2(r_{\theta=0})+S^2(r_{\theta=0})\right]}}. \quad (18.32)$$

Here, the arguments of the Fresnel integrals are calculated for $\varphi = 90°$:

$$r_1 = \sqrt{\frac{\beta}{\pi R_0}}\left(-\frac{B}{2} - R_0\frac{\beta B}{2}\sin\theta\right),$$
$$r_2 = \sqrt{\frac{\beta}{\pi R_0}}\left(+\frac{B}{2} - R_0\frac{\beta B}{2}\sin\theta\right), \tag{18.33}$$

and

$$r_{\theta=0} = r_2(\theta=0) = \frac{B}{2}\sqrt{\frac{\beta}{\pi R_0}}. \tag{18.34}$$

Similar to the *H*-plane sectoral horn, the principal *E*-plane pattern can be accurately calculated if no approximation of the phase distribution is made. Then, the function $f_E(\theta)$ has to be calculated by numerical integration of (compare with (18.20))

$$f_E(\theta) \propto \int_{-B/2}^{B/2} e^{-j\beta\sqrt{R_0^2+y'^2}} e^{j\beta\sin\theta\cdot y'} dy'. \tag{18.35}$$

E- AND H-PLANE PATTERN OF E-PLANE SECTORAL HORN

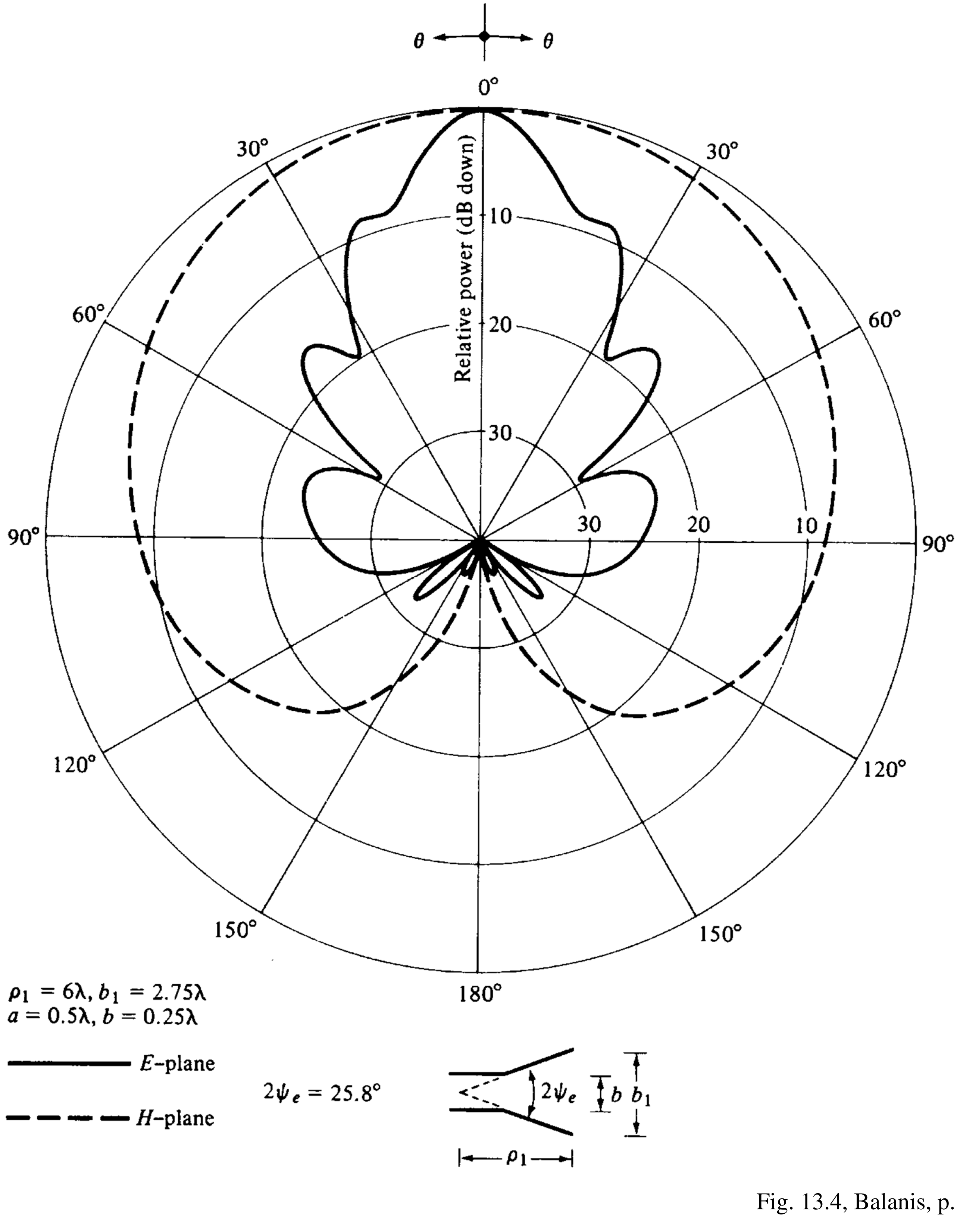

Fig. 13.4, Balanis, p. 660

Directivity

The directivity of the E-plane sectoral horn is found in a manner analogous to the H-plane sectoral horn:

$$D_E = \frac{a}{\lambda}\frac{32}{\pi}\frac{B}{\lambda}\varepsilon_{ph}^E = \frac{4\pi}{\lambda^2}\varepsilon_t\varepsilon_{ph}^E aB\,, \tag{18.36}$$

where

$$\varepsilon_t = \frac{8}{\pi^2},\ \varepsilon_{ph}^E = \frac{C^2(q)+S^2(q)}{q^2},\ \ q = \frac{B}{\sqrt{2\lambda R_0}}.$$

A family of universal directivity curves $\lambda D_E / a$ vs. B/λ with R_0 being a parameter is given below.

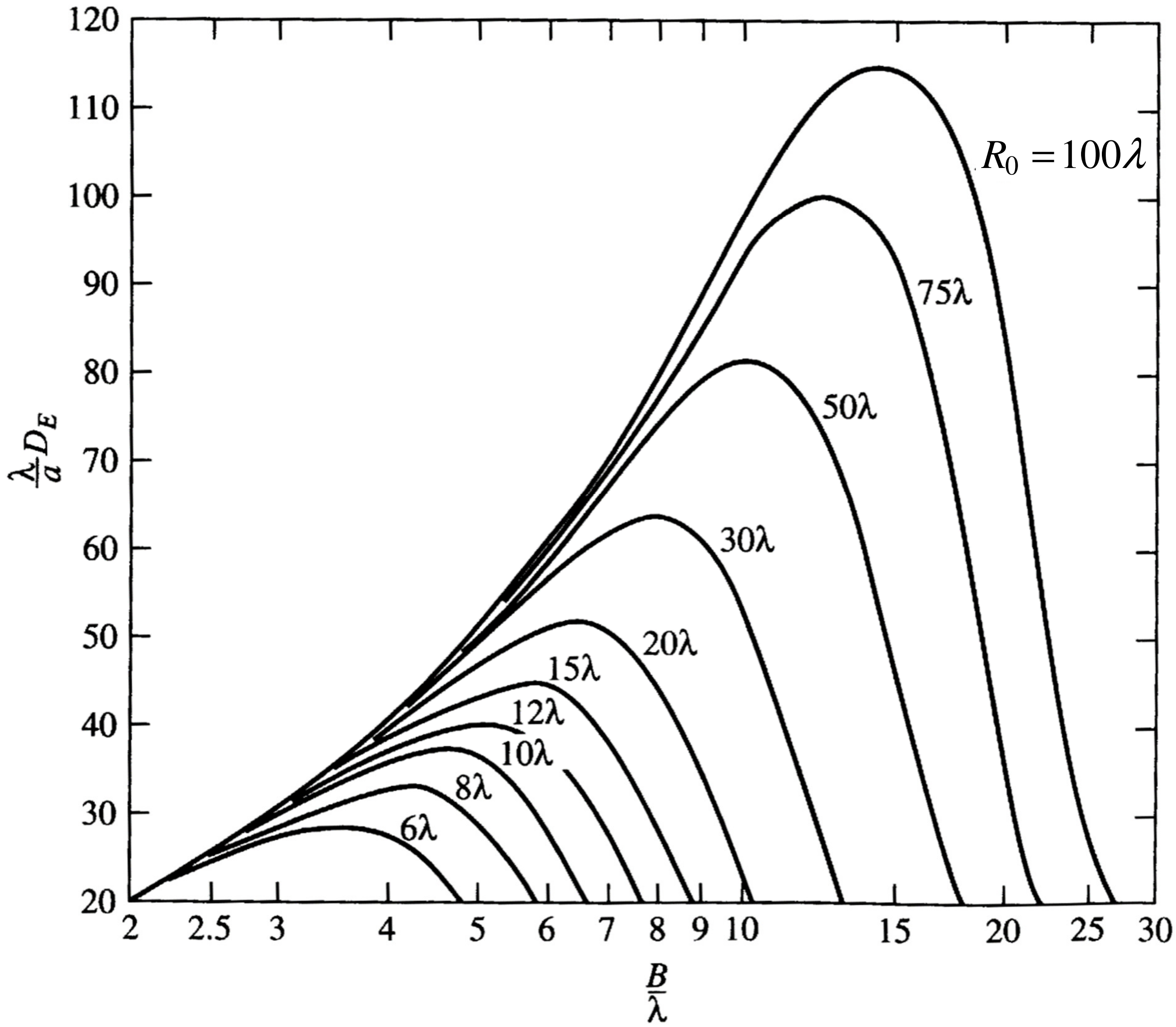

[Stutzman&Thiele, *Antenna Theory and Design*]

The optimal relation between the flared height B and the horn apex length R_0 that produces the maximum possible directivity is

$$B = \sqrt{2\lambda R_0}\,. \tag{18.37}$$

1.3 The pyramidal horn

The pyramidal horn is a very popular antenna in the microwave frequency ranges (from ≈ 1 GHz to 30 GHz). The feeding waveguide is flared in both directions, the E-plane and the H-plane. All results are combinations of the E-plane sectoral horn and the H-plane sectoral horn analyses. The field distribution at the aperture is approximated as

$$E_{a_y} \approx E_0 \cos\left(\frac{\pi}{A}x\right) e^{-j\frac{\beta}{2}\left(\frac{x^2}{R_0^{E2}}+\frac{y^2}{R_0^{H2}}\right)}. \tag{18.38}$$

The E-plane principal pattern of the pyramidal horn is the same as the E-plane principal pattern of the E-plane sectoral horn. The same holds for the H-plane patterns of the pyramidal horn and the H-plane sectoral horn.

The directivity of the pyramidal horn can be found by introducing the phase efficiency factors of both planes and the taper efficiency factor of the H-plane:

$$D_P = \frac{4\pi}{\lambda^2}\varepsilon_t \varepsilon_{ph}^E \varepsilon_{ph}^H AB\,, \tag{18.39}$$

where

$$\varepsilon_t = \frac{8}{\pi^2};$$

$$\varepsilon_{ph}^H = \frac{\pi^2}{64t}\left\{\left[C(p_1)-C(p_2)\right]^2 + \left[S(p_1)-S(p_2)\right]^2\right\};$$

$$p_1 = 2\sqrt{t}\left[1+\frac{1}{8t}\right],\quad p_2 = 2\sqrt{t}\left[-1+\frac{1}{8t}\right],\ t = \frac{1}{8}\left(\frac{A}{\lambda}\right)^2 \frac{1}{R_0^H/\lambda};$$

$$\varepsilon_{ph}^E = \frac{C^2(q)+S^2(q)}{q^2},\quad q = \frac{B}{\sqrt{2\lambda R_0^E}}.$$

The gain of a horn is usually very close to its directivity because the radiation efficiency is very good (low losses). The directivity as calculated with (18.39) is very close to measurements. The assumed field distribution in the horn aperture is a physical optics approximation, which does not take into account only multiple diffractions and the diffraction at the edges of the horn. However, these phenomena, which are unaccounted for, lead to only very minor fluctuations of the measured results about the prediction of (18.39). That is why horns are often used as ***gain standards*** in antenna measurements.

The optimal directivity of an E-plane horn is achieved at $q = 1$ [see also (18.37)], $\varepsilon_{ph}^{E} = 0.8$. The optimal directivity of an H-plane horn is achieved at $t = 3/8$ [see also (18.24)], $\varepsilon_{ph}^{H} = 0.79$. Thus, the optimal horn has a phase aperture efficiency of

$$\varepsilon_{ph}^{P} = \varepsilon_{ph}^{H}\varepsilon_{ph}^{E} = 0.632. \qquad (18.40)$$

The total aperture efficiency includes the taper factor, too:

$$\varepsilon_{ph}^{P} = \varepsilon_{t}\varepsilon_{ph}^{H}\varepsilon_{ph}^{E} = 0.81 \cdot 0.632 = 0.51. \qquad (18.41)$$

Therefore, the best achievable directivity for a rectangular waveguide horn is about half that of a uniform rectangular aperture.

We reiterate that best accuracy is achieved if ε_{ph}^{H} and ε_{ph}^{E} are calculated numerically without using the second-order phase approximation as in (18.38).

Optimum horn design

Usually, the optimum (from the point of view of maximum gain) design of a horn is desired because it results in the shortest axial length for a given gain. The whole design can be actually reduced to the solution of a single fourth-order equation. For a horn to be realizable, the following must be true:

$$R_E = R_H = R_P. \qquad (18.42)$$

The figures below summarize the notations used in describing the horn's geometry.

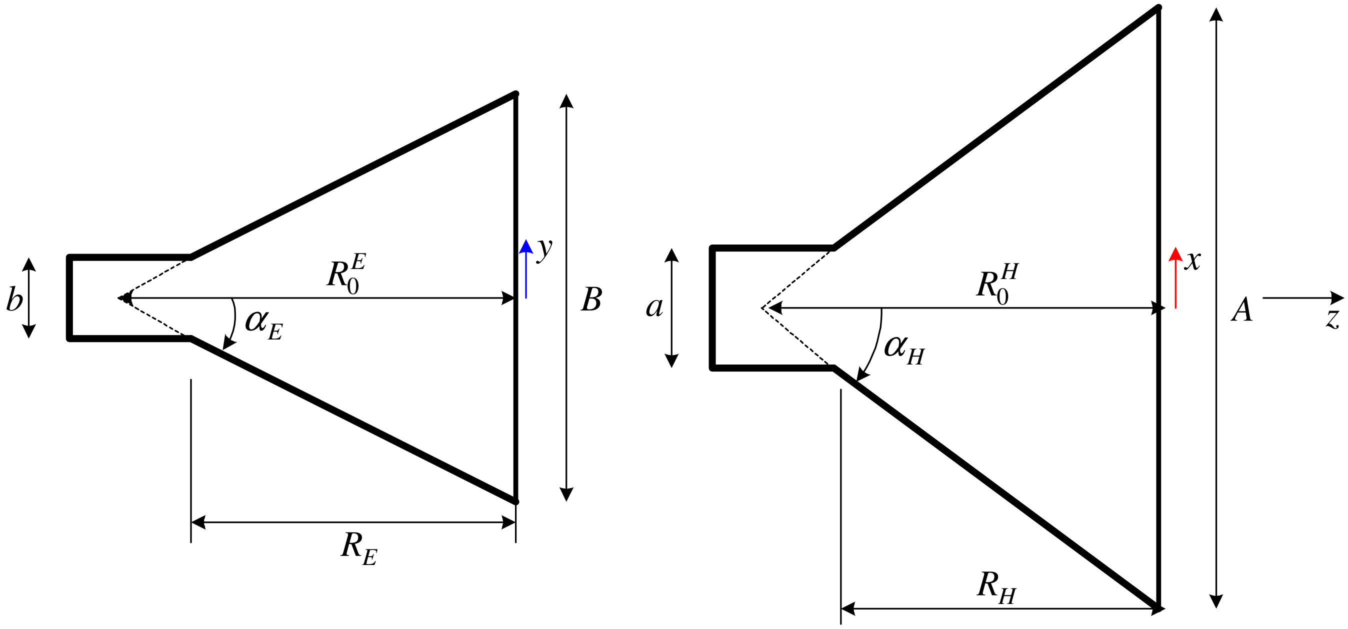

It can be shown that

$$\frac{R_0^H}{R_H} = \frac{A/2}{A/2 - a/2} = \frac{A}{A-a}, \tag{18.43}$$

$$\frac{R_0^E}{R_E} = \frac{B/2}{B/2 - b/2} = \frac{B}{B-b}. \tag{18.44}$$

The optimum-gain condition in the *E*-plane (18.37) is substituted in (18.44) to produce

$$B^2 - bB - 2\lambda R_E = 0. \tag{18.45}$$

There is only one physically meaningful solution to (18.45):

$$B = \frac{1}{2}\left(b + \sqrt{b^2 + 8\lambda R_E}\right). \tag{18.46}$$

Similarly, the maximum-gain condition for the *H*-plane of (18.24) together with (18.43) yields

$$R_H = \frac{A-a}{A}\left(\frac{A^2}{3\lambda}\right) = A\frac{(A-a)}{3\lambda}. \tag{18.47}$$

Since $R_E = R_H$ must be fulfilled, (18.47) is substituted in (18.46), which gives

$$B = \frac{1}{2}\left(b + \sqrt{b^2 + \frac{8A(A-a)}{3}}\right). \tag{18.48}$$

Substituting in the expression for the horn's gain,

$$G = \frac{4\pi}{\lambda^2}\varepsilon_{ap} AB, \tag{18.49}$$

gives the relation between A, the gain G, and the aperture efficiency ε_{ap}:

$$G = \frac{4\pi}{\lambda^2}\varepsilon_{ap} A \frac{1}{2}\left(b + \sqrt{b^2 + \frac{8A(a-a)}{3}}\right), \tag{18.50}$$

$$\Rightarrow A^4 - aA^3 + \frac{3bG\lambda^2}{8\pi\varepsilon_{ap}} A - \frac{3G^2\lambda^4}{32\pi^2\varepsilon_{ap}^2} = 0. \tag{18.51}$$

Equation (18.51) is the optimum pyramidal horn design equation. The optimum-gain value of $\varepsilon_{ap} = 0.51$ is usually used, which makes the equation a fourth-order polynomial equation in A. Its roots can be found analytically (which is not particularly easy) and numerically. In a numerical solution, the first guess is usually set at $A^{(0)} = 0.45\lambda\sqrt{G}$. Once A is found, B can be computed from (18.48) and $R_E = R_H$ is computed from (18.47).

Sometimes, an optimal horn is desired for a known axial length R_0. In this case, there is no need for nonlinear-equation solution. The design procedure follows the steps: (a) find A from (18.24), (b) find B from (18.37), and (c) calculate the gain G using (18.49) where $\varepsilon_{ap} = 0.51$.

Horn antennas operate well over a bandwidth of 50%. However, gain performance is optimal only at a given frequency. To understand better the frequency dependence of the directivity and the aperture efficiency, the plot of these curves for an X-band (8.2 GHz to 12.4 GHz) horn fed by WR90 waveguide is given below ($a = 0.9$ in. = 2.286 cm and $b = 0.4$ in. = 1.016 cm).

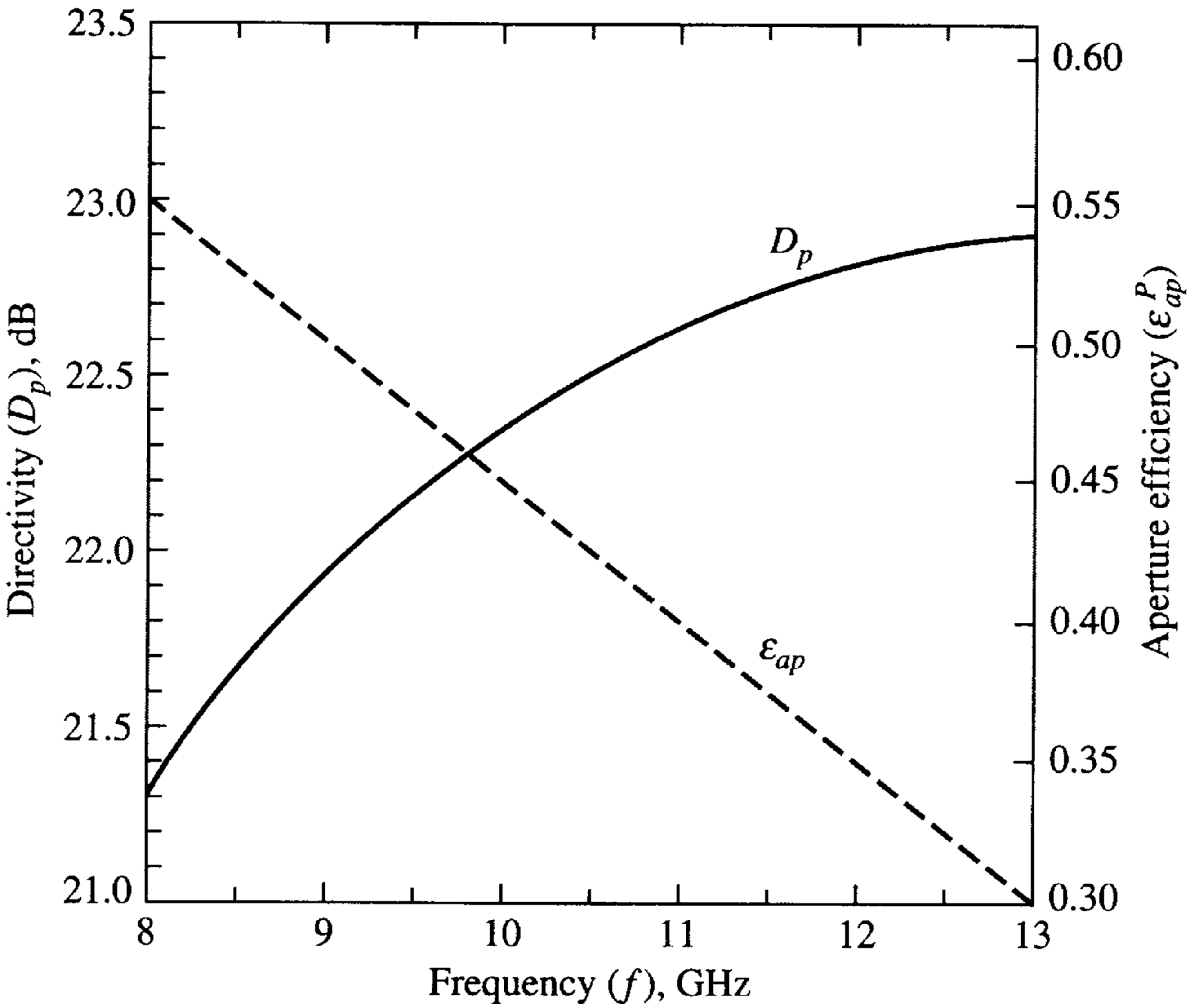

[Stutzman&Thiele, *Antenna Theory and Design*]

The gain increases with frequency, which is typical for aperture antennas. However, the curve shows saturation at higher frequencies. This is due to the decrease of the aperture efficiency, which is a result of an increased phase difference in the field distribution at the aperture.

The pattern of a “large” pyramidal horn ($f = 10.525$ GHz, feed is waveguide WR90):

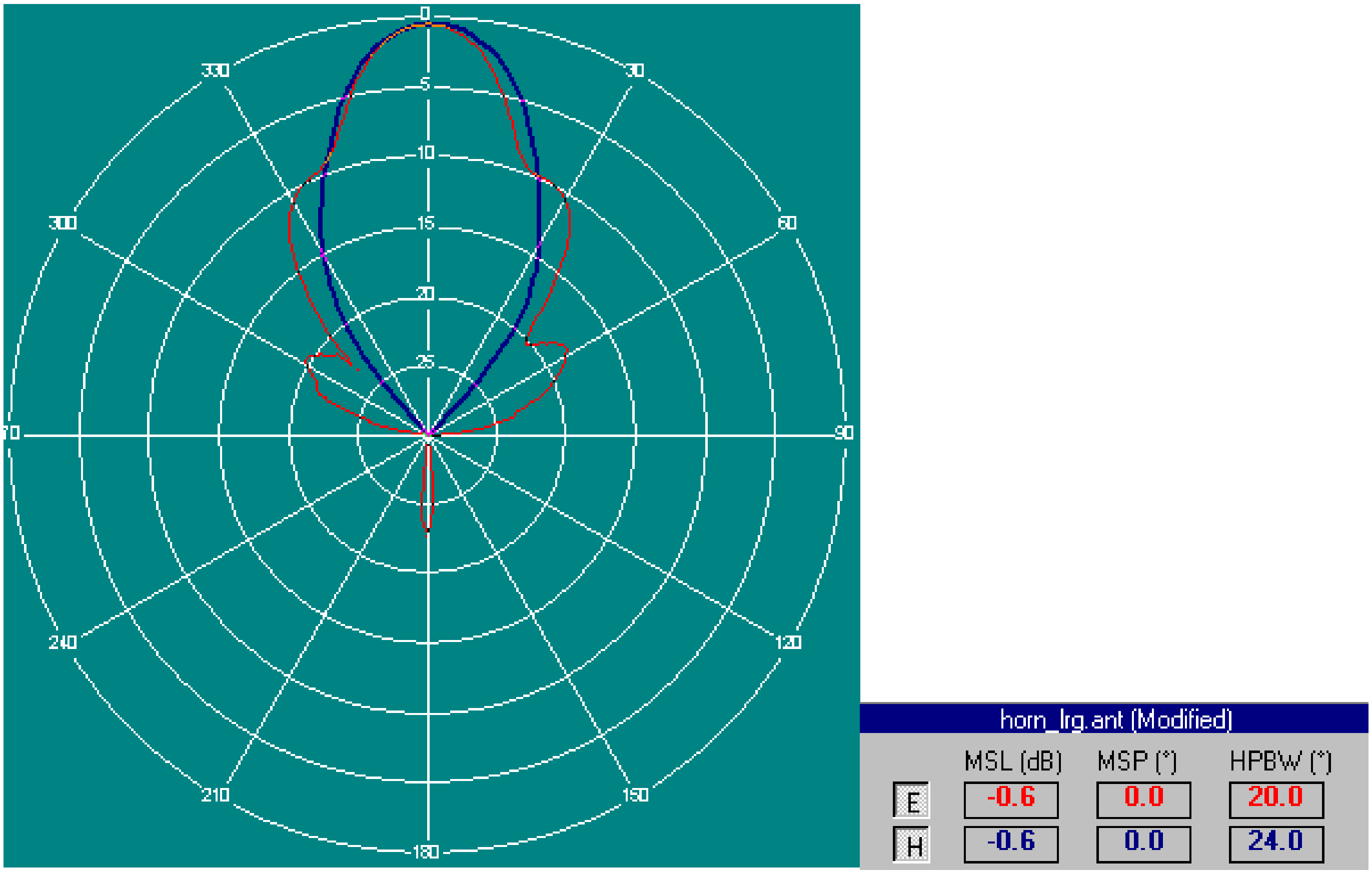

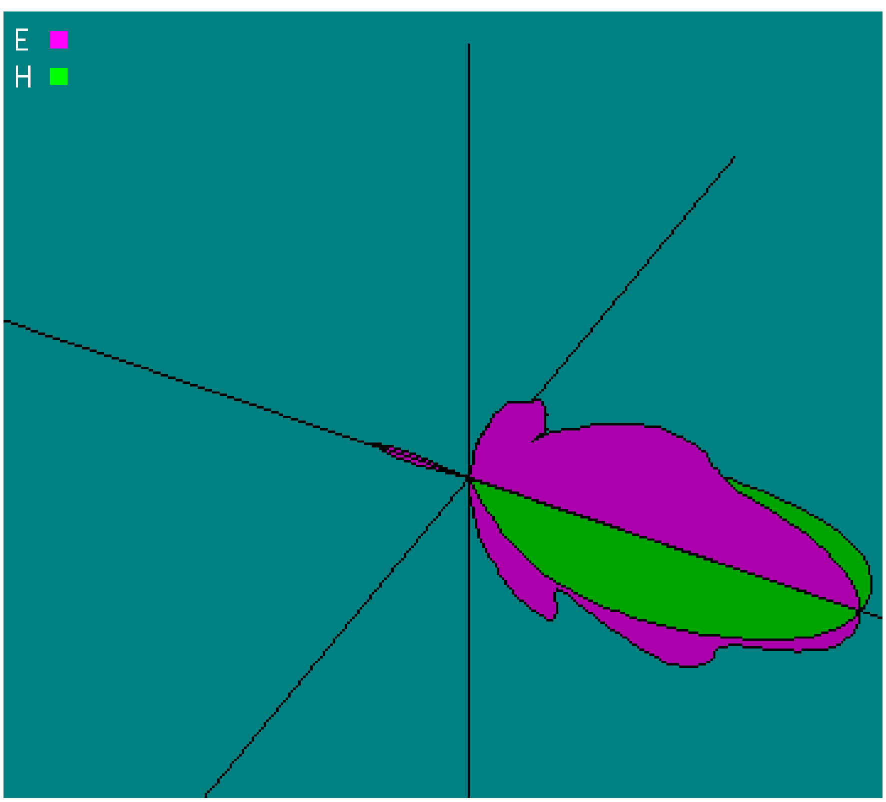

Comparison of the *E*-plane patterns of a waveguide open end, "small" pyramidal horn and "large" pyramidal horn:

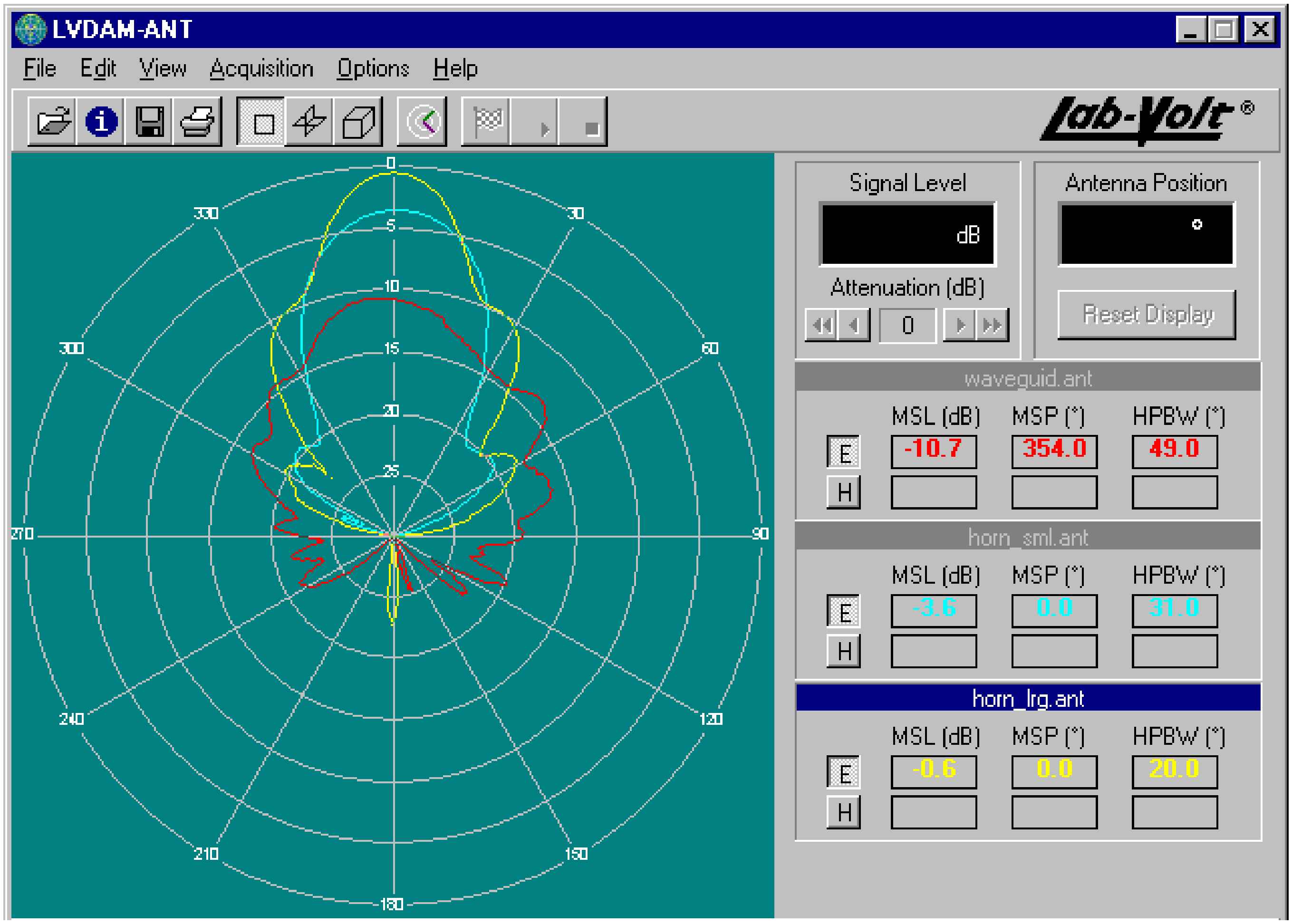

Note the multiple side lobes and the significant back lobe. They are due to diffraction at the horn edges, which are perpendicular to the **E** field. To reduce edge diffraction, enhancements are proposed for horn antennas such as

- corrugated horns
- aperture-matched horns

The corrugated horns achieve tapering of the **E** field in the vertical direction, thus, reducing the side-lobes and the diffraction from the top and bottom edges. The overall main beam becomes smooth and nearly rotationally symmetrical (esp. for $A \approx B$). This is important when the horn is used as a feed to a reflector antenna.

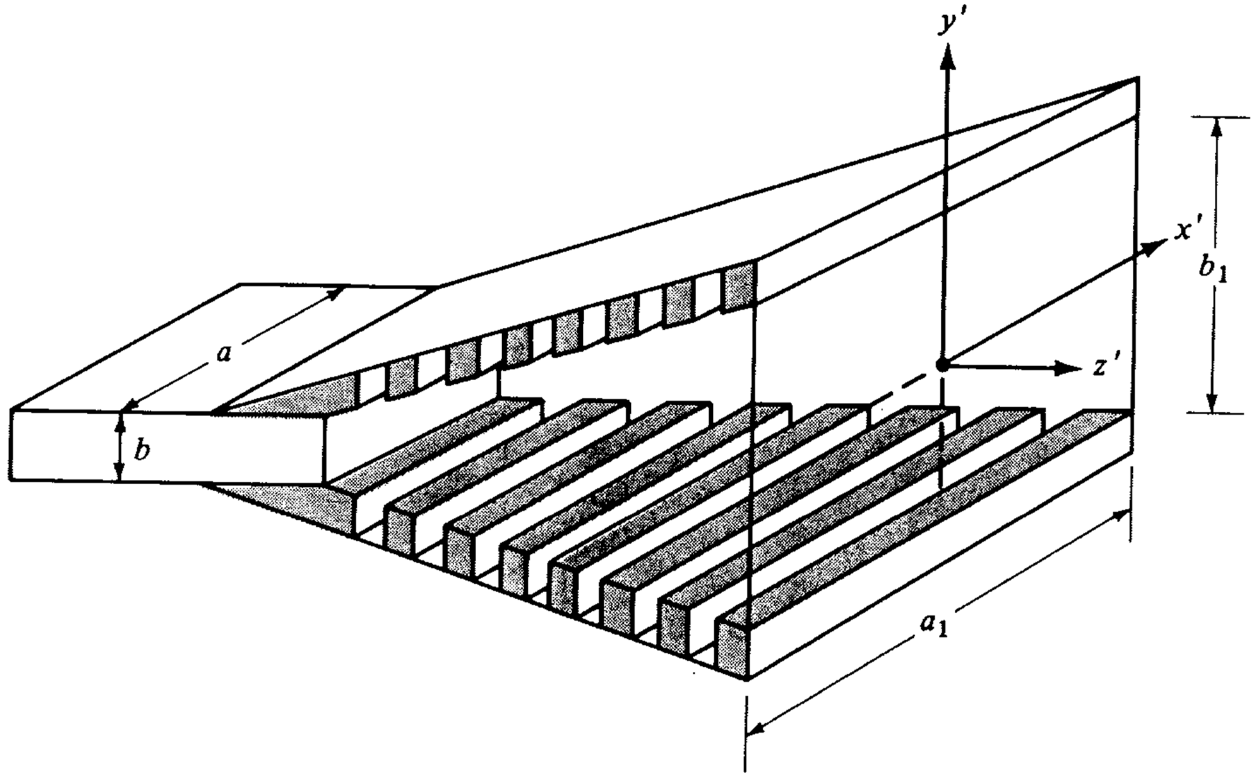

y'
x'
b1
a
z'
b
a1

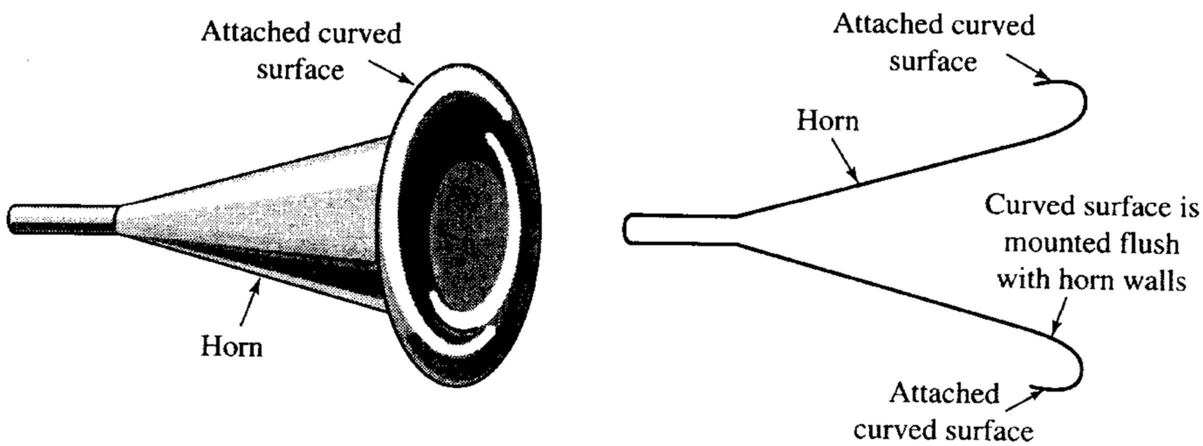

Attached curved surface
Horn
Attached curved surface
Horn
Curved surface is mounted flush with horn walls
Attached curved surface

Comparison of the *H*-plane patterns of a waveguide open end, "small" pyramidal horn and "large" pyramidal horn:

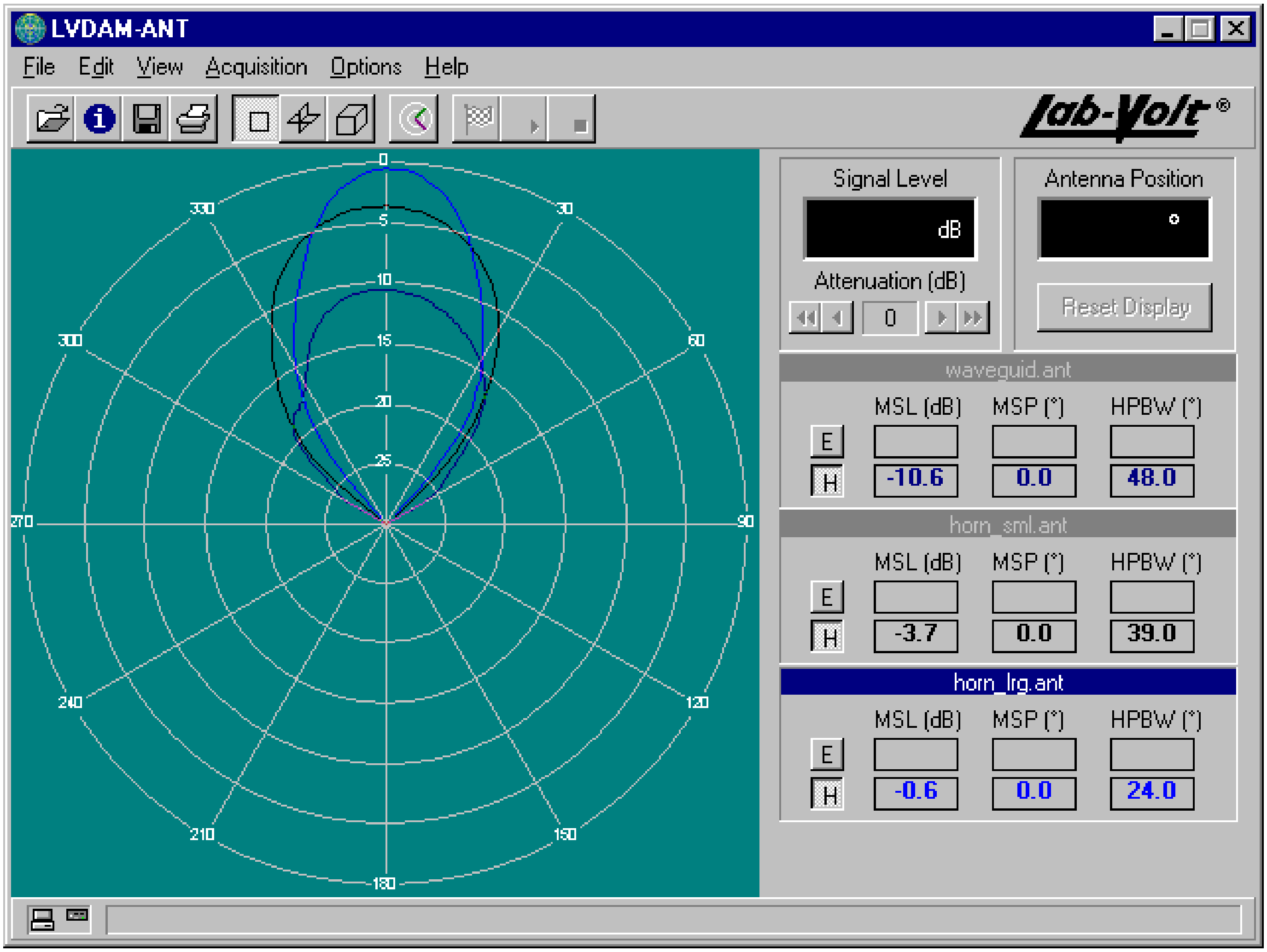

2 Circular apertures

2.1 A uniform circular aperture

The uniform circular aperture is approximated by a circular opening in an infinite ground plane illuminated by a uniform plane wave normally incident from behind.

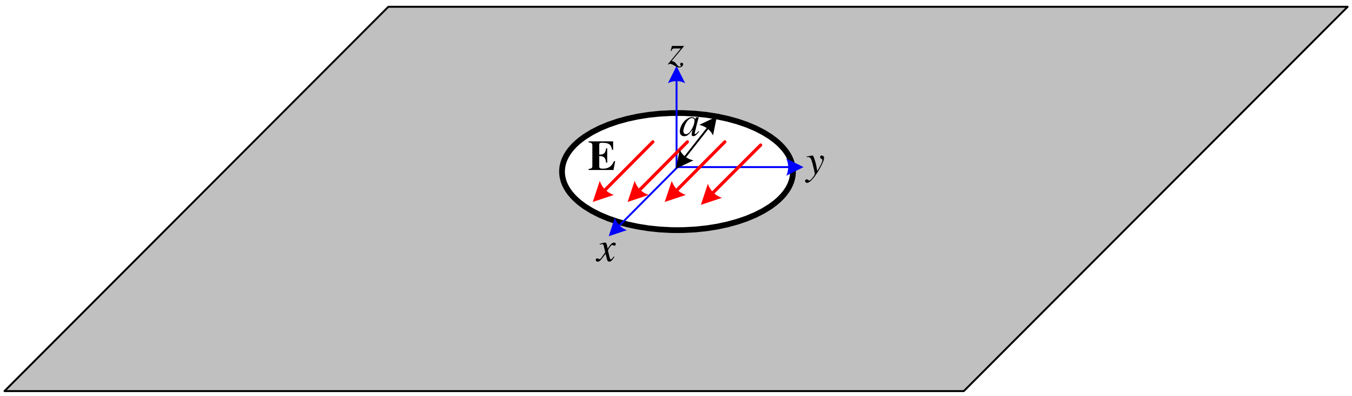

The idealized field distribution is described as

$$\mathbf{E}_a = \hat{\mathbf{x}} E_0, \quad \rho' \le a. \tag{18.52}$$

The radiation integral is

$$I_x^E = E_0 \iint_{S_a} e^{j\beta \hat{\mathbf{r}} \cdot \mathbf{r}'} ds'. \tag{18.53}$$

The integration point is at

$$\mathbf{r}' = \hat{\mathbf{x}} \rho' \cos\varphi' + \hat{\mathbf{y}} \rho' \sin\varphi'. \tag{18.54}$$

In (18.54), cylindrical coordinates are used. In spherical coordinates,

$$\hat{\mathbf{r}} \cdot \mathbf{r}' = \rho' \sin\theta (\cos\varphi \cos\varphi' + \sin\varphi \sin\varphi') = \rho' \sin\theta \cos(\varphi - \varphi') . \tag{18.55}$$

Hence, (18.53) is written as

$$I_x^E = E_0 \int_0^a \left[\int_0^{2\pi} e^{j\beta\rho' \sin\theta \cos(\varphi - \varphi')} d\varphi' \right] \rho' d\rho' = 2\pi E_0 \int_0^a \rho' J_0(\beta \rho' \sin\theta) d\rho'. \tag{18.56}$$

Here, $J_0(\cdot)$ is the Bessel function of the first kind of order zero. Applying the identity

$$\int xJ_0(x)dx = xJ_1(x) \tag{18.57}$$

to (18.56) leads to

$$I_x^E = 2\pi E_0 \frac{a}{\beta \sin\theta} J_1(\beta a \sin\theta). \tag{18.58}$$

Note that in this case the equivalent magnetic current formulation of the equivalence principle is used [see Lecture 17]. The far field is obtained as

$$\begin{aligned}\mathbf{E} &= \left(\hat{\boldsymbol{\theta}}\cos\varphi - \hat{\boldsymbol{\varphi}}\cos\theta\sin\varphi\right) j\beta \frac{e^{j\beta r}}{2\pi r} I_x^E = \\ &= \left(\hat{\boldsymbol{\theta}}\cos\varphi - \hat{\boldsymbol{\varphi}}\cos\theta\sin\varphi\right) j\beta E_0 \pi a^2 \frac{e^{j\beta r}}{2\pi r} \frac{2J_1(\beta a \sin\theta)}{\beta a \sin\theta}.\end{aligned} \tag{18.59}$$

<u>Principal-plane patterns</u>

***E*-plane** $(\varphi = 0)$: $\quad E_\theta(\theta) = \dfrac{2J_1(\beta a \sin\theta)}{\beta a \sin\theta}$ (18.60)

***H*-plane** $(\varphi = 90°)$: $\quad E_\varphi(\theta) = \cos\theta \cdot \dfrac{2J_1(\beta a \sin\theta)}{\beta a \sin\theta}$ (18.61)

The 3-D amplitude pattern:

$$\overline{E}(\theta,\varphi) = \sqrt{1-\sin^2\theta\sin^2\varphi} \cdot \underbrace{\frac{2J_1(\beta a \sin\theta)}{\beta a \sin\theta}}_{f(\theta)} \tag{18.62}$$

The larger the aperture, the less significant the $\cos\theta$ factor is in (18.61) because the main beam in the $\theta = 0$ direction is very narrow and in this small solid angle $\cos\theta \approx 1$. Thus, the 3-D pattern of a large circular aperture features a fairly symmetrical beam.

Example plot of the principal-plane patterns for $a = 3\lambda$:

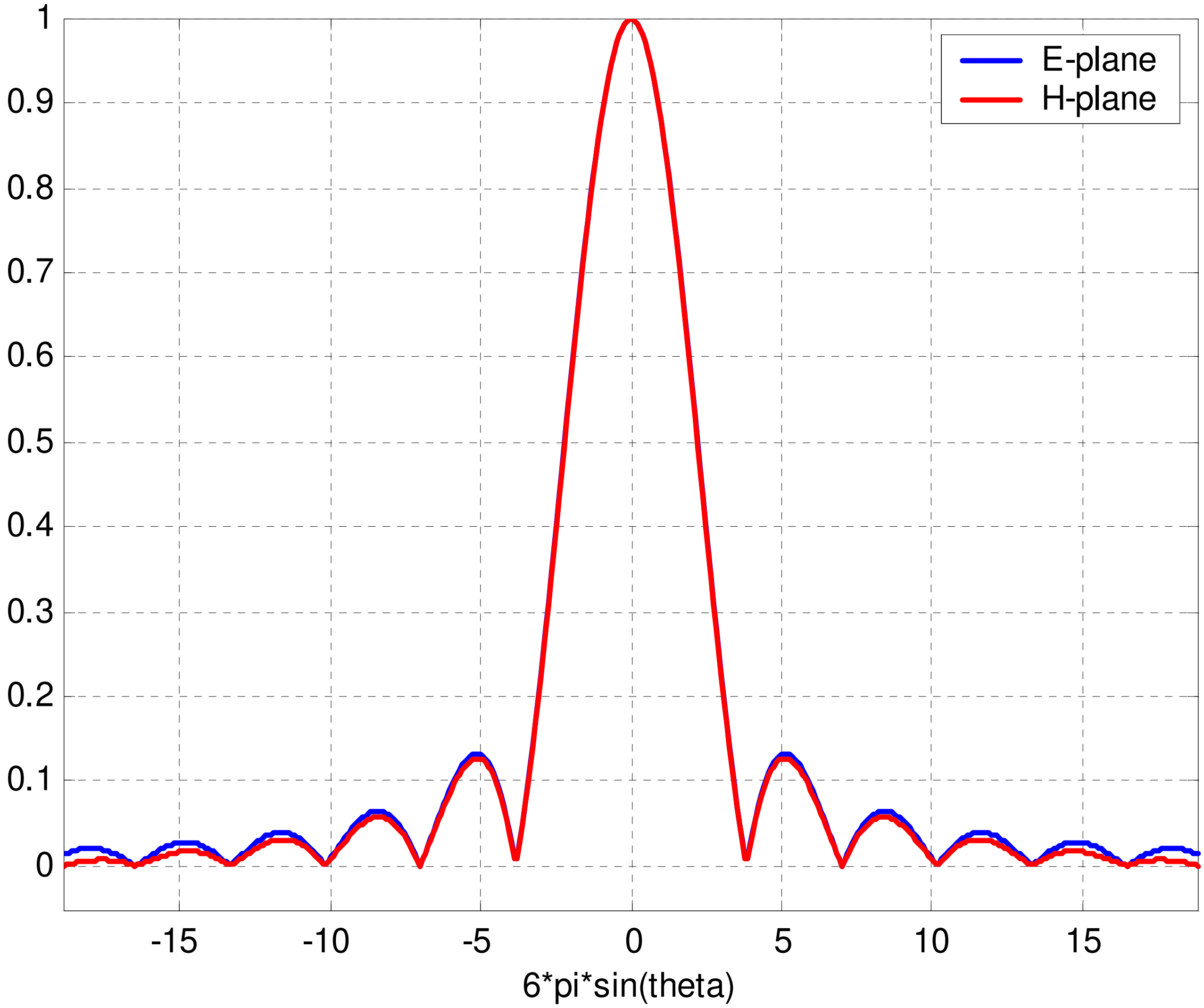

The half-power angle for the $f(\theta)$ factor is obtained at $\beta a \sin\theta \approx 1.6$. So, the HPBW for large apertures ($a \gg \lambda$) is given by

$$HPBW = 2\theta_{1/2} \approx 2\arcsin\left(\frac{1.6}{\beta a}\right) \approx 2\frac{1.6}{\beta a} = 58.4\frac{\lambda}{2a}, \text{ deg.} \qquad (18.63)$$

For example, if the diameter of the aperture is $2a = 10\lambda$, then $HPBW = 5.84°$.

The side-lobe level of any uniform circular aperture is 0.1332 (-17.5 dB).

Any *uniform* aperture has unity taper aperture efficiency, and its directivity can be found directly in terms of its physical area,

$$D_u = \frac{4\pi}{\lambda^2} A_p = \frac{4\pi}{\lambda^2} \pi a^2. \qquad (18.64)$$

2.2 Tapered circular apertures

Many practical circular aperture antennas can be approximated as radially symmetric apertures with field amplitude distribution, which is tapered from the center toward the aperture edge. Then, the radiation integral (18.56) has a more general form:

$$I_x^E = 2\pi \int_0^a E_0(\rho')\rho' J_0(\beta\rho'\sin\theta)d\rho' . \tag{18.65}$$

In (18.65), we still assume that the field has axial symmetry, i.e., it does not depend on φ'. Often used approximation is the parabolic taper of order *n*:

$$E_a(\rho') = E_0\left[1-\left(\frac{\rho'}{a}\right)^2\right]^n \tag{18.66}$$

where E_0 is a constant. This is substituted in (18.65) to calculate the respective component of the radiation integral:

$$I_x^E(\theta) = 2\pi E_0 \int_0^a \left[1-\left(\frac{\rho'}{a}\right)^2\right]^n \rho' J_0(\beta\rho'\sin\theta)d\rho' . \tag{18.67}$$

The following relation is used to solve (18.67):

$$\int_0^1 (1-x^2)^n x J_0(bx)dx = \frac{2^n n!}{b^{n+1}} J_{n+1}(b) . \tag{18.68}$$

In our case, $x = \rho'/a$ and $b = \beta a \sin\theta$. Then, $I_x^E(\theta)$ reduces to

$$I_x^E(\theta) = E_0\left(\frac{\pi a^2}{n+1}\right) f(\theta,n) , \tag{18.69}$$

where

$$f(\theta,n) = \frac{2^{n+1}(n+1)! J_{n+1}(\beta a\sin\theta)}{\left(\beta a\sin\theta\right)^{n+1}} \tag{18.70}$$

is the normalized pattern (neglecting the angular factors such as $\cos\varphi$ and $\cos\theta\sin\varphi$).

The aperture taper efficiency is calculated to be

$$\varepsilon_t = \frac{\left[C + \dfrac{1-C}{n+1}\right]^2}{C^2 + \dfrac{2C(1-C)}{n+1} + \dfrac{(1-C)^2}{2n+1}}. \tag{18.71}$$

Here, C denotes the *pedestal height*. The pedestal height is the edge field illumination relative to the illumination at the center.

The properties of several common tapers are given in the tables below. The parabolic taper ($n=1$) provides lower side lobes in comparison with the uniform distribution ($n=0$) but it has a broader main beam. There is always a trade-off between low side-lobe levels and high directivity (small HPBW). More or less optimal solution is provided by the parabolic-on-pedestal aperture distribution. Moreover, this distribution approximates very closely the real case of circular reflector antennas, where the feed antenna pattern is intercepted by the reflector only out to the reflector rim.

a. Parabolic taper

$$E_a(\rho') = \left[1 - \left(\frac{\rho'}{a}\right)^2\right]^n$$

$$f(\theta, n) = \frac{2^{n+1}(n+1)!J_{n+1}(\beta a \sin\theta)}{(\beta a \sin\theta)^{n+1}}$$

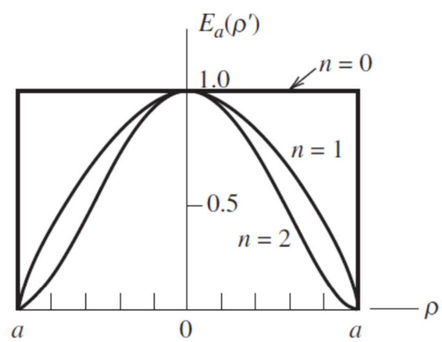

n	HP (rad)	Side Lobe Level (dB)	ε_t	Normalized Pattern $f(\theta, n)$	Distribution
0	$1.02\dfrac{\lambda}{2a}$	−17.6	1.00	$\dfrac{2J_1(\beta a \sin\theta)}{\beta a \sin\theta}$	Uniform
1	$1.27\dfrac{\lambda}{2a}$	−24.6	0.75	$\dfrac{8J_2(\beta a \sin\theta)}{(\beta a \sin\theta)^2}$	Parabolic
2	$1.47\dfrac{\lambda}{2a}$	−30.6	0.55	$\dfrac{48J_3(\beta a \sin\theta)}{(\beta a \sin\theta)^2}$	Parabolic squared

[Stutzman&Thiele]

b. Parabolic taper on a pedestal

$$E_a(\rho') = C + (1-C)\left[1 - \left(\frac{\rho'}{a}\right)^2\right]^n$$

$$f(\theta, n, C) = \frac{Cf(\theta, n=0) + \dfrac{1-C}{n+1} f(\theta, n)}{C + \dfrac{1-C}{n+1}}$$

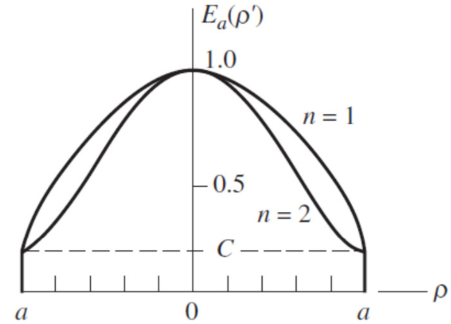

Edge Illumination		$n = 1$			$n = 2$		
C_{dB}	C	HP (rad)	Side Lobe Level (dB)	ε_t	HP (rad)	Side Lobe Level (dB)	ε_t
−8	0.398	$1.12\frac{\lambda}{2a}$	−21.5	0.942	$1.14\frac{\lambda}{2a}$	−24.7	0.918
−10	0.316	$1.14\frac{\lambda}{2a}$	−22.3	0.917	$1.17\frac{\lambda}{2a}$	−27.0	0.877
−12	0.251	$1.16\frac{\lambda}{2a}$	−22.9	0.893	$1.20\frac{\lambda}{2a}$	−29.5	0.834
−14	0.200	$1.17\frac{\lambda}{2a}$	−23.4	0.871	$1.23\frac{\lambda}{2a}$	−31.7	0.792
−16	0.158	$1.19\frac{\lambda}{2a}$	−23.8	0.850	$1.26\frac{\lambda}{2a}$	−33.5	0.754
−18	0.126	$1.20\frac{\lambda}{2a}$	−24.1	0.833	$1.29\frac{\lambda}{2a}$	−34.5	0.719
−20	0.100	$1.21\frac{\lambda}{2a}$	−24.3	0.817	$1.32\frac{\lambda}{2a}$	−34.7	0.690

[Stutzman&Thiele]